J Mater Sci (2010) 45:3160–3168
DOI 10.1007/s10853-010-4322-x

Design of composite porous cermets synthesized by hydrothermal treatment of CrAl powder followed by calcination

Serguei Tikhov · Vladimir Usoltsev · Aleksey Salanov · Sergey Tsybulya · Yurii Chesalov · Galina Kustova · Vladislav Sadykov · Galina Golubkova · Oleg Lomovskii

Received: 30 June 2009 / Accepted: 13 February 2010 / Published online: 4 March 2010

Abstract The microstructure of the porous Cr–Al metal–oxide cermet was studied by means of XRD, SEM, EDX as well as IR and Raman spectroscopy. This cermet was synthesized by mechanical alloying of Cr–Al powders in an AGO-2 planetary ball mill followed by hydrothermal treatment in a special stainless steel die and calcination in air. As a result, a highly porous monolith comprised of metal-like particles randomly distributed in the oxide matrix (Cr_2O_3 and Al_2O_3) was formed. Two types of the composite cores were found in cermets. The first one consisted of chromium phase containing nanoparticles sized from 50 to 140 nm and Al-enriched phase at the interfaces. The second one consisted of new chromium oxide phases with hexagonal Cr_2N-like and fcc CrN-like structures probably with Cr_2O and CrO stoichiometry. These new phases were stabilized within aggregates of the nanocomposite particles containing inclusions of alumina. The relations between different preparation stages and the cermet microstructure are discussed.

S. Tikhov (✉) · V. Usoltsev · A. Salanov · S. Tsybulya · Y. Chesalov · G. Kustova · V. Sadykov
Boreskov Institute of Catalysis SB RAS, Lavrentieva Str., 5, Novosibirsk, Russia 630090
e-mail: tikhov@catalysis.ru

S. Tsybulya · V. Sadykov · O. Lomovskii
Novosibirsk State University, Pirogova Str., 2, Novosibirsk, Russia 630090

G. Golubkova · O. Lomovskii
Institute of Solid State Chemistry and Mechanochemistry SB RAS, Kutateladze Str., 18, Novosibirsk, Russia 630128

Introduction

Oxide matrix cermets are used in various sectors of industry due to their thermomechanical and dielectric properties [1]. Highly porous cermets prepared from powder CrAl alloys are promising materials for catalyst supports, membranes and filter materials. Synthesis of cermets includes a number of unusual steps. First, powder alloys were prepared by high-energy mechanical alloying of aluminium and chromium mixture under air. Mechanical treatment provide interaction between chromium and aluminium eventually leading to formation of amorphous Cr_4Al and Cr_2Al phases with alloying time increasing [2]. Then, powdered alloys were partially oxidized under hydrothermal conditions. Strong porous monoliths were formed after calcination in air. In general, thermal treatment conditions used for synthesis of cermets are much milder than are essential for porometals preparation by hot pressing and high-temperature sintering [1]. Cermets have developed macroporous structure with pore sizes from 1 to 100 μm. However, unlike porometals that have similar macroporous structure, cermets additionally have developed mesoporous structure located in their oxide component. Furthermore, the metal particles are evenly distributed in this mesoporous matrix. So, the contacts between particles of the porous materials are oxide-like rather than metal-like. Their mechanical, thermo-physical and textural properties are largely determined by the ratio between ceramic and metal components, requiring additional studies.

The textural and catalytic properties of cermets based on powder CrAl alloys prepared by hydrothermal treatment followed by calcination were described earlier [3]. Meanwhile, problems of the ceramic component type in cermet, quantitative relations between ceramic and metal

components and their spatial distribution in the monoliths were still a matter of discussion. Initially, it was suggested that $Al_{86}Cr_{14}$ intermetallides were formed in cermets [3]. However, several researchers observed chromium nitrides after calcination of Fe and Cr alloys in air at high temperatures [4–6]. More detailed studies of the chromium nitrides synthesis in nitrogen or ammonia showed that the presence of oxygen even in trace amounts in nitrogen-containing environment led to formation of mixed chromium oxynitrides [7, 8]. In this paper, we present detailed design of CrAl alloy based cermet as a result of structural, spectral and microstructural studies.

Experimental

Materials

Commercial grade aluminium (GOST 5499-71, not less than 99.5 wt% Al) and high purity chromium (99.9 wt% Cr) powders were used.

Synthesis

The monolith preparation procedure included next steps:

(a) Mechanical alloying (MA) of the powdered metal blend containing 80 wt% of chromium and 20 wt% of aluminium was carried out using AGO-2 high-power planetary ball mill. Alloying times were 3, 5 and 10 min. The acceleration of balls was 600 m/s^2. The weight ratio of balls to powder was 200:10 and ball diameter was 5 mm. An X-ray amorphous Cr_4Al phase and a weakly crystallized Cr_2Al intermetallide phase were formed during the mechanical alloying. Some chromium remained as a metallic phase.

(b) Then, the blend was loaded into a stainless steel die specially constructed to ensure free access of water. The die with Cr–Al blend was placed in boiling water (hydrothermal treatment) and kept there for 4 h producing a strong monolith. During the hydrothermal treatment aluminium hydroxides were formed on the surface of the alloy particles. They cemented powder at the places of contact to form porous monolith.

(c) The granulated product was removed from die, dried for 1 h at 120 °C and calcined under air with the temperature slowly increasing up to 1100 °C. The calcination yielded strong material (cermet). At this stage the hydroxides were decomposed and the alloy components interacted with each other and the components of the air.

Characterization

The phase composition was studied by XRD using a URD-63 diffractometer with CuKα radiation. Special computer program POLYCRYSTAL was used to determine precisely unit cell parameters of Cr, CrN and Cr_2N phases. The average size (L) of chromium particles was calculated using the Scherer equation:

$$L(\mathrm{Cr}) = \frac{\alpha}{\beta \cdot \cos\theta},$$

where α is the wavelength, β is the half-width of diffraction peak and θ is the angle of reflection.

SEM micrographs were obtained using JEOL JSM-6460LV scanning electron microscope equipped with energy-dispersive X-ray analyzer EDX-INCA/Energy-350 (Oxford Inst.) for point measurements. Cermet cross-section was made by sealing into epoxy and polishing. The accelerating voltage used for registration of the TEM images and EDX analysis of large surface segments with dimensions $35 \times 45 = 1.6\ 10^3$ μm^2 (Fig. 4) was equal to 25 keV. Smaller surface fragments were analysed by EDX using the accelerating voltage of 10 keV, which allowed us to analyse fragments with dimensions 0.5–1.5 μm. The values of atomic concentrations obtained after the standard computer processing included decimal values. The data reported in Table 2 were rounded to integer values. However, the actual error in the determination of the atomic concentrations in certain points, including the differences in the dimensions of the analysis regions for the light and heavy elements, may be substantially higher, probably, as high as 10–20 at.%. The approximate stoichiometry of chromium oxides was estimated assuming that aluminium oxide had $AlO_{1.5}$ stoichiometry (Al_2O_3). The FTIR spectra were registered using a BOMEM MB-102 spectrometer in the frequency range 4000–250 cm^{-1} with 4 cm^{-1} resolution. The samples for FTIR experiments were prepared by pressing 1.5 mg of cermet with 500 mg KBr into a pellet. The Raman spectra were registered using a Bruker RFS 100/S FT-Raman spectrometer. The 1064 nm line of Nd-YAG laser with 100 mW powder was used as the excitation source. The mechanical strength was measured using a Prochnometr PK-2 instrument for pellets (diameter—10 mm, height—3 mm). The porosity (ε) was calculated from apparent and real densities of material.

Results and discussion

Crystalline phases according to XRD

According to the X-ray diffraction data (Fig. 1), Cr–Al cermet mainly consists of chromium, chromia (α-Cr_2O_3)

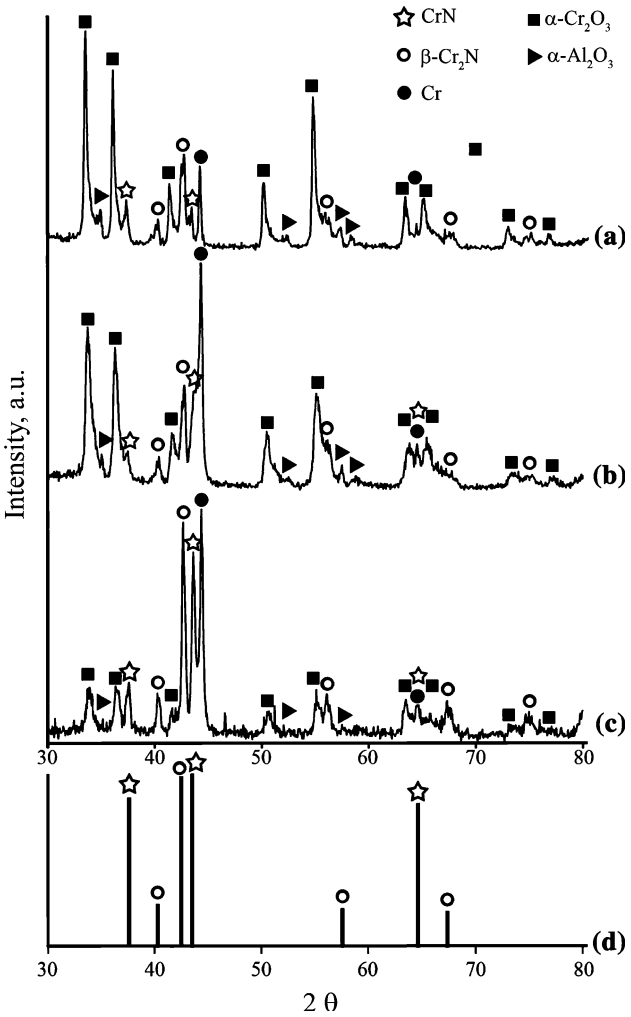

Fig. 1 XRD patterns of cermets synthesized from Cr–Al (20 wt%) blend with different alloying time: (*a*) 3 min, (*b*) 5 min, (*c*) 10 min, (*d*) JCPDS data for CrN and Cr_2N type structures

and alumina (α-Al_2O_3) phases as well as chromium nitride-like phases ('CrN', 'Cr_2N'). After longer MA, the intensities of the peaks attributed to the chromium and 'nitride-like' phases increase in comparison to those of chromium oxide (Fig. 1). The unit cell parameters calculated from experimental data and literature data for face-centred cubic chromium collected in Table 1. Experimental value is close to literature, so chromium phase is free from aluminium [9]. The unit cell parameters calculated from the diffraction data for hexagonal 'Cr_2N' lattice ($a = b = 4.815$; $c = 4.470$) and face-centred cubic lattice typical for 'CrN' ($a = b = c = 4.155$) are quite different from the literature data. The reported values are $a = b = 4.8113$; $c = 4.4841$ for the Cr_2N phase and $a = b = c = 4.140$ for the CrN phase [10, 11]. The comparison of relative intensities of peaks attributed to the nitride-like phase and Cr^0 with intensities of the Cr_2O_3 and Al_2O_3 peaks suggests that concentration of former phases

Table 1 The experimental and literature values of unit cell parameters and coherently scattering domain of the chromium phase in the cermet with different alloying time of Cr–Al powder

Sample, τ_{MA}	Unit cell parameters (Å)	Coherently scattering domain (Å)	
		(110)	(200)
3 min	$a = b = c = 2.893 \pm 1$	1031	1393
5 min	$a = b = c = 2.888 \pm 1$	682	653
10 min	$a = b = c = 2.888 \pm 1$	597	475
Reference	$a = b = c = 2.884$ [8]	–	–

in the cermet is significantly higher especially for the cermet prepared after 10 min MA.

Microstructure analysis

According to SEM data (Fig. 2), sample consists of particles with different size and shape. The particles themselves are non-uniform as well. It was found that shell of the particles forming cermet consists of aluminium and chromium oxides. The stoichiometry of chromium oxides varies from CrO_3 to Cr_2O_3 (Table 2, Shell). The spaces between particles form open macropores with dimensions from one to tens micrometres. The oxides form continuous matrix surrounding evenly distributed composite cores. Note that the data on the Cr:Al and CrO_x stoichiometry reported in Table 2 are approximate and reflect only the main trends in the compositions of the certain cermet fragments that are discussed in the text.

Two dominating types of submicron particles are distinguished in the polished cuts. The particles of first type are evidently nanocomposite with chaotically mixed light and dark spots (Fig. 2b). The other particles are much more homogeneous and have rounded internal pores with diameters about 1 μm (Fig. 2c). The particles of both types have a shell clearly separated from core and Al:Cr ratio—1:2 ÷ 1:1.5 (Table 2). Meanwhile, the shell of the 'homogeneous' particles has a subsurface layer (Table 2, Point 6) that is considerably different from the surface one (Table 2c, Point 6) and has much lower chromium concentration (Al:Cr—1:0.5). The two-layer type of coating is also preserved at places of contacts between particles and contacts with pores (Figs. 2c, 3c).

The core compositions of two types are substantially different. The core of the 'homogeneous' particles has no oxygen and large excess of chromium relative to aluminium (Al:Cr—1:5, 1:6, Fig. 3c; Table 2, Points 7, 8). Some voids inside 'homogeneous' metal core are also observed. The core of the 'nanocomposite' particles is characterized by gradual decrease of the oxygen concentration from the subsurface regions to the centre from $CrO_{1.5}$ to $CrO_{1.1}$ and

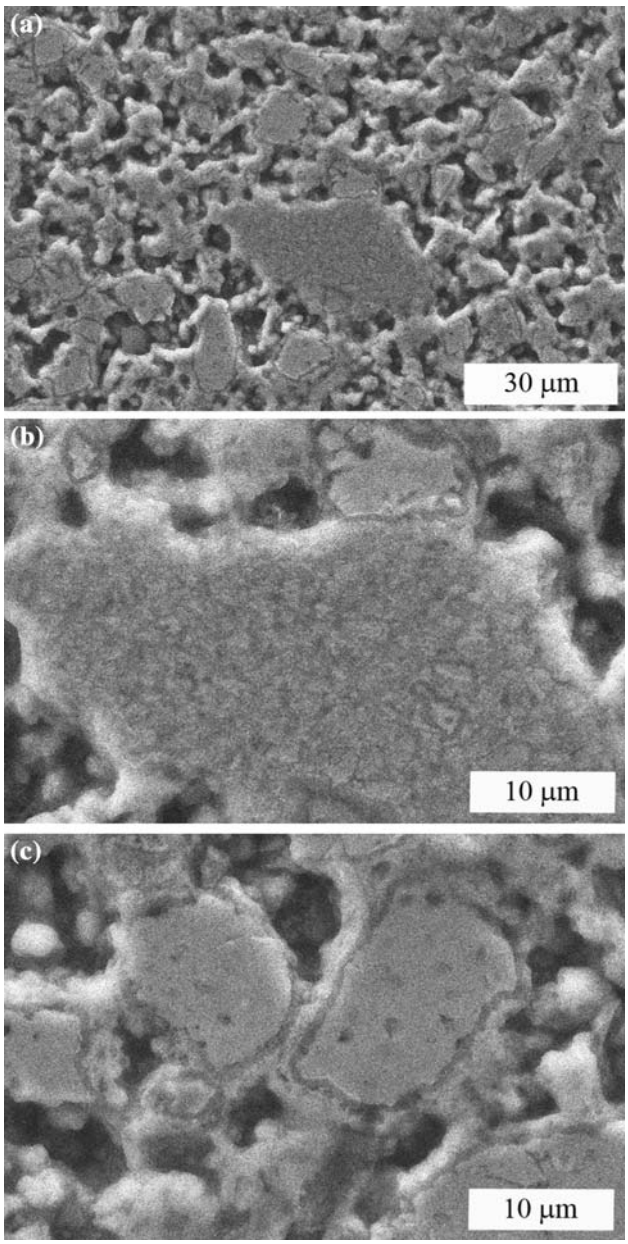

Fig. 2 SEM micrographs of different parts of cermet: (**a**) general view, (**b**) 'nanocomposite' particle, (**c**) 'homogeneous' particle

$CrO_{0.4}$ (Fig. 3a, b; Table 2; Points 2, 3, 4).The ratio between metals is almost constant (Al:Cr—1:2). However, the darker spots have lower chromium concentrations (Fig. 3; Table 2, Point 3). At the centre of some 'nanocomposite' cores no oxygen has been observed. Note that the absolute values in the stoichiometry of certain components in the microstructure can vary depending on the EDX analysis conditions. However, there are main tendencies that are preserved. One of them is the lack of oxygen in the 'homogeneous' particles. The oxygen concentration in all the 'nanocomposite' particles tends to be lower closer to the centre of the 'core'. Also, the compositions of the surface and subsurface layers of the oxide matrix are different. It is these tendencies rather than the absolute values that will be discussed below.

During the analysis of the cermet chemical composition by EDX we were surprised to find out that the samples did not contain significant amounts of nitrogen (Fig. 4). The detailed analysis of chemical composition also did not reveal nitrogen (Table 2). However, we carried out EDX analysis of commercial nitrides AlN_3 and BN where the nitride phases predominate according to XRD and IR spectroscopy of lattice vibrations. A well pronounced peak of nitrogen was observed in the spectra at the same analysis conditions in accordance with the XRD data [8, 12].

FTIR and Raman studies

The FTIR and Raman spectra of cermet are presented in Fig. 5a, b. The spectra correspond to IR and Raman spectra of α-Cr_2O_3 with the main peaks at 630 and 580 cm^{-1} [13, 14]. Minor differences in the frequencies and relative intensities of absorption bands are apparently related to the presence of alumina in chromium oxide. The absorption band at 890 cm^{-1} in the FTIR spectrum might reflect the presence of Cr(VI) ions [12]. The bands at frequencies below 500 cm^{-1} are notably widened. According to literature data, such changes in the spectra of ionic crystals can be explained by their fine dispersity or non-stoichiometric composition, i.e. the presence of oxygen vacancies [15, 16].

Absorption bands and Raman lines that could be reliably attributed to vibrations of chromium nitrides were not observed in registered FTIR and Raman spectra. According to the literature data [7, 17], intense wide absorption line with maximum at 550 cm^{-1} is observed in the FTIR spectra of chromium nitrides. This line was not observed in spectra of cermet sample.

Bulk content of 'nanocomposite' cores: nitrides or oxides?

The discrepancy between XRD data suggesting that phases with the structure of nitrides formed after high-temperature treatment in air and spectral data proving formation of chromium oxides is an important feature of obtained results. The spectral methods show that chromium oxides predominate in the cermet. According to EDX data, stoichiometry of bulk oxide phases is close to CrO_1 or Cr_2O (although $CrO_{1.5}$ was also observed). Hence, the FTIR data indicates that Cr_2O_3 is the predominating phase.

Earlier, conclusions about formation of chromium nitrides in chromium alloys with iron were based exclusively on XRD data [4]. XPS data were also discussed [6] but no actual spectra were presented. Most other researchers report that nitrogen concentration in chromium

Table 2 Chemical contents and appropriate stoichiometry of the different fragments of cermet according to EDX data (Fig. 3)

Fragments (picture)	Place	Points of analysis	Content (at.%)			Al:Cr	CrO_x[a]
			O	Al	Cr		
'Nanocomposite' particles (a, b)	Shell	1	72	10	18	~1:2	CrO_3
	Core	2	59	13	28	~1:2	$CrO_{1.4}$
		3	56	17	27	~1:1.5	$CrO_{1.1}$
		4	42	16	42	~1:2	$CrO_{0.4}$
'Homogenous' particles (c)	Shell/contact	5	58	15	27	~1:2	$CrO_{1.3}$
		6	60	25	15	~1:0.5	$CrO_{1.5}$
	Core	7	11	15	74	~1:5	–
		8	0	15	85	~1:6	–

Accelerating voltage is 10 keV

[a] Supposing stoichiometry of Al_2O_3:$AlO_{1.5}$

oxides formed in the intergranular space of particles is very low (less than 1 at.%) [18]. However, these results were obtained only for forged plates or rods rather than powders. The formation of chromium nitride, CrN, was proved both by structural and spectral methods only for thin chromium films treated in nitrogen [7]. Still, according to XPS data, the film contained up to 50 at.% O. The authors made a conclusion about formation of oxynitride with chromium nitride structure suggesting that both substances (oxide and nitride) have similar structures. It should be noted that there are almost no structural data on ordered chromium oxide phases with Cr/O ratio smaller than 1.5. The reported data on CrO phase [19] are considerably different from our data (Table 3). Orthorhombic structures with approximate stoichiometry Cr_6O_{15} and Cr_5O_{12} were also described [20]. However, both their structure and stoichiometry substantially differ from ones observed by us. Also, there is discrepancy between experimental intensities of obtained diffraction peaks for different interplanar spacing and published data for chromium nitrides (Table 3) [8, 9]. So, obtained results lead us to the conclusion that nitride-like Cr(II) and Cr(I) oxides are formed under our conditions (powder alloys prepared by mechanical alloying followed by hydrothermal treatment and calcination at high temperature in air).

Note that no spectral information on the structures with CrO or Cr_2O stoichiometry is available. So, the widening of the absorption bands at frequencies below 500 cm^{-1} might be caused by such structures where the octahedral coordination of chromium with oxygen atoms is preserved.

'Homogeneous' cores: where is the aluminium located?

As mentioned above, presence of well-crystallized chromium metal core is typical for the 'homogeneous' particles of the chromium–aluminium cermet. Meanwhile, the EDX data show that these cores contain significant amounts of aluminium. However, it is well known [1] that aluminium is very poorly soluble in the chromium lattice. Also, unit cell parameters of chromium in the cermets calculated from XRD data are close to known for pure chromium (Table 1). This result suggests that aluminium is mostly located between chromium grains. Indeed, average crystalline size of chromium particles (~480–1400 Å, Table 1) is much smaller than the dimensions of 'homogeneous' particles determined by SEM as well as the size of the regions analysed by EDX. Probably, aluminium observed by EDX is located at the boundaries of these grains as alloy with chromium. The same was proposed for FeAl alloys formed under mechanical alloying [21].

The other question concerns the void formation in cermet particles. During calcination at high temperature part of aluminium can be segregated on the surface and oxidized. It results in formation of a protective thin oxide film on the surface similar to that formed in FeCrAl alloys, which substantially improves the stability of such particles to bulk oxidation [22]. This process can explain the enrichment of aluminium in oxide sublayer for 'homogeneous' cores (Fig.3c; Table 2). Also, this redistribution of aluminium-containing phases between volume and surface as well as the formation of X-ray invisible (probably—two-dimentional) Cr_4Al or Cr_2Al phases located at grain boundaries, can result in formation of the large pores inside the 'homogeneous' cores. The formation of some ordered Cr_4Al or Cr_2Al phases from amorphous ones have been proposed earlier based on thermal analysis data [2].

Cermet design

As already mentioned, the cermet microstructure is characterized by two types of cores covered by oxide film (Fig. 6). In 'nanocomposite' cores the aluminium concentration is approximately constant whereas oxygen concentration gradually decreases towards the centre. This changes stoichiometry from CrO_3 at the surface to $CrO_{\sim 0}$ near centre of the particles. Apparently, layered structure of 'nanocomposite' with aluminium oxide regions alternating with the regions enriched with chromium in different oxidation states suppresses oxygen diffusion from surface towards the centre and prevents chromium from oxidation

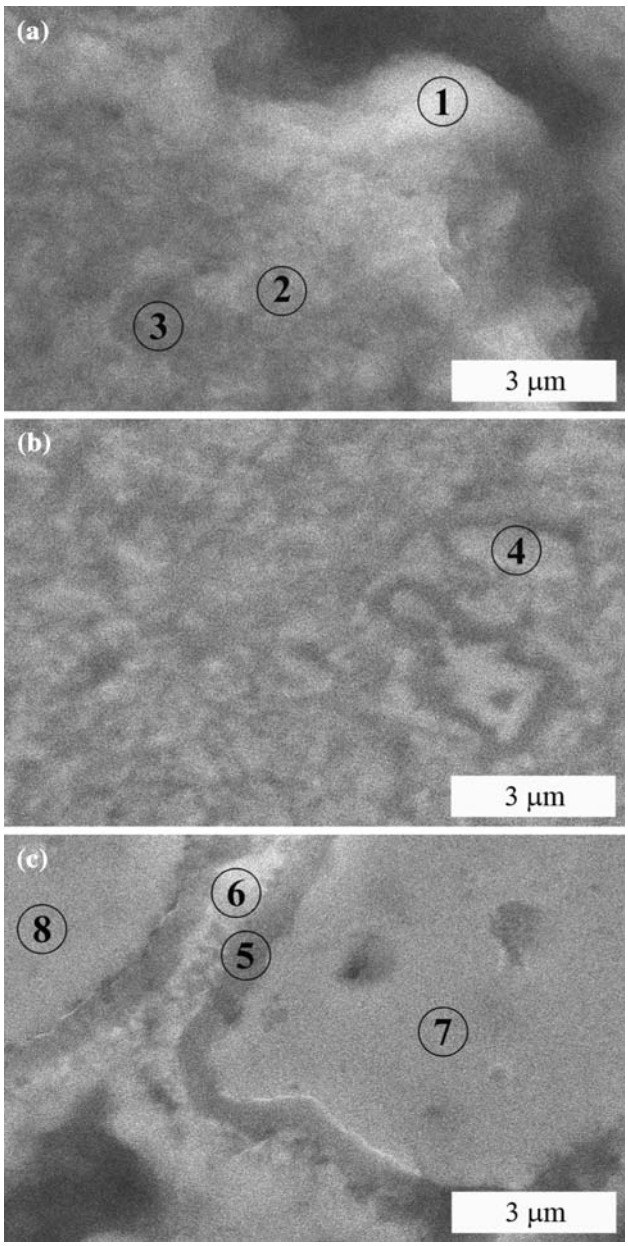

Fig. 3 SEM micrographs of different parts of cermet: **a**, **b** 'nanocomposite' particle; **c** 'homogeneous' particles. Different points of EDX analysis are numerated (See Table 2): (*1*) shell of 'nanocomposite' particle; (*2*), (*3*), (*4*) core of 'nanocomposite' particle from edge to centre; (*5*), (*6*) shell/contact of 'homogeneous' particles; (*7*), (*8*) cores of 'homogeneous' particles. The analysis was carried out using the accelerating voltage 10 keV. The size of the analysis regions is approximately equal to that of the selected areas

to Cr_2O_3 at high temperatures. The dimensions of such 'nanograins' are substantially smaller than the effective size of spots analyzed by EDX. So, these 'nanograins' cannot be analyzed individually. Thus, it is the 'nanocomposite' structure of the particles that can lead to the formation of nitride-like phases similar to observed for thin films [7].

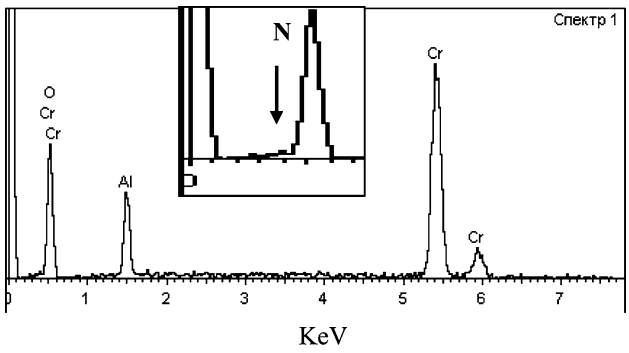

Fig. 4 EDX spectrum of the polished cermet obtained from an area $35\times 45 = 1.6 \times 10^3$ μm^2. Accelerating voltage is 25 keV

The 'homogeneous' cores consist of chromium metal grains divided by aluminium enriched boundaries. These boundaries are, probably, CrAl intermetallides with amorphous or two-dimensional structure.

The synthesised cermet has fairly high porosity ~42%. It is somewhat higher than in porometals prepared by pressing and high-temperature calcination [23]. The fraction of pores larger than 10 μm in the total pore volume is rather high also (Figs. 2a, 3a). In our case external pressure was not applied for powder filling during the cermet synthesis. So, average dimensions of pores in the cermets are larger. Relatively low bulk density of the cermet monolith ~3 g/cm^3 compared to chromium metal is due to both high porosity and the contribution of chromium and aluminium oxides. The mechanical strength of the cermet (~20 MPa) is lower than that of porometals because mechanically strong contacts between the particles in cermets have oxide nature. However, it is still higher than that of traditional porous oxide ceramics.

Main stages of the cermet preparation and their relation to the cermet microstructure

(1) Mechanical alloying. As it was shown above based on the XRD and differential dissolution data, MA successively leads to the formation of amorphous and weakly crystallized Cr_4Al and Cr_2Al phases [2] in agreement with the general principles of mechanical alloying for metal systems [24, 25]. In addition, the mean dimensions of the powdered particles decrease. The obtained information on the specific features of the structure and microstructure allowed us to understand better the processes taking place during MA. First, MA undoubtedly makes both the metal particles and the grains smaller. This tendency is reflected in the gradual decrease of the mean crystallite size with the MA time (Table 1). Second, the amorphous phases are predominantly localized at the boundaries of the grains. It is natural to assume that

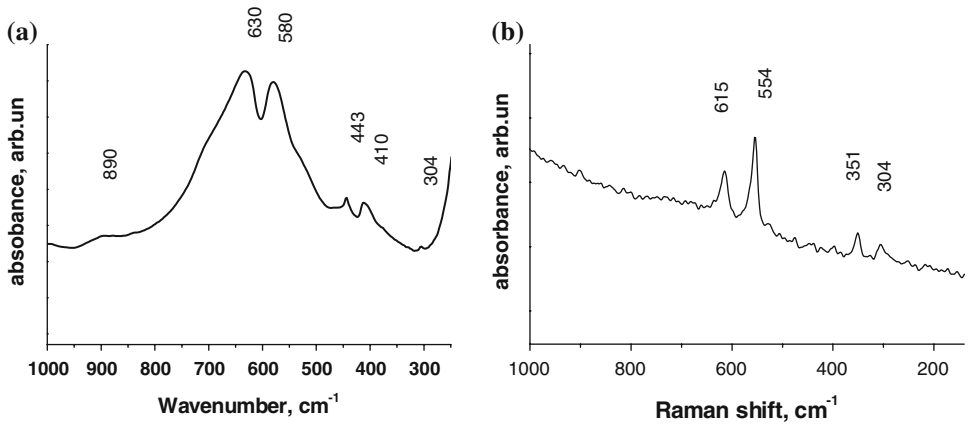

Fig. 5 FTIR (**a**) and Raman (**b**) spectra of the cermet

Table 3 Diffraction parameters for sample with 10 min mechanical alloying with references

hkl	'Cr_2O'		Cr_2N [9]		hkl	'CrO'		CrN [10]		hkl	CrO [19]	
	d_{hkl}	I_{hkl}	d_{hkl}	I_{hkl}		d_{hkl}	I_{hkl}	d_{hkl}	I_{hkl}		d_{hkl}	I_{hkl}
110	2.407	9	2.4056	15	111	2.393	22	2.394	80	–	2.44	10
002	2.242	12	2.2419	21	200	2.076	100	2.068	100	–	2.26	10
111	2.121	100	2.1200	100	220	1.462	29	1.463	80	–	2.04	10
112	1.642	32	1.6404	19	–	–	–	–	–	–	1.90	30

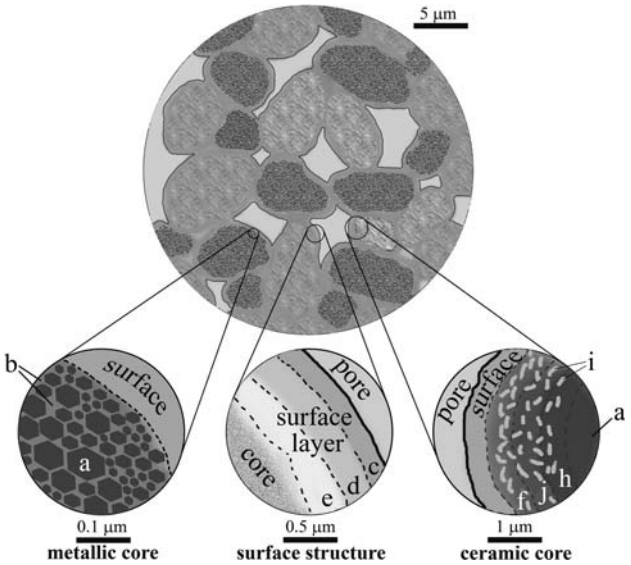

Fig. 6 Multiscale model of the porous Cr–Al-based cermet: *a* CrO grains, *b* $CrAl_x$ intermetallides at the grain boundaries; *c*, *d*, *e* surface oxide layers with different composition; *f*, *g*, *h* CrO_x with nitride structure; *i* alumina

the two types of the particles observed in the cermets correspond to the two types of particles formed during MA. The particles of one type are formed in the processes described earlier [1] that are accompanied by the densification of the aggregates. The particles of the second type are looser and appear to be something like nanocomposites consisting of chromium and amorphous aluminium particles. These two types of particles form two types of cores during the cermet formation under the oxidative treatments. Most likely, the loose particles are formed first, followed by the denser particles. However, according to the XRD data obtained for the cermets (Fig. 1), the relative amounts of the cores belonging to the two types (chromium and nitride-like phases) grow in parallel. So, either the formation of these two particle types is very slow or the two types are formed during MA in independent parallel processes. Also, the loose particles might result from the aggregation of the nanoparticles after their size reduction [26]. These hypotheses need additional studies for verification.

(2) Hydrothermal treatment. The hydrothermal treatment cements the metal particles into a mechanically strong monolith. The surface of the aluminium metal particles is oxidized by water to form various hydrated products that stay at the places of contact between the aggregates and glue them [3, 27]. Apparently, the first surface oxide layer is formed due to the interaction of the particle surface with water (Fig. 3d; Table 2, 'Shell'). The amorphous aluminium particles included into the loose nanocomposites mentioned above might also undergo partial oxidation.

(3) Calcination. The high-temperature calcination in air results in dehydration of the hydrothermal oxidation products and deeper oxidation of the metal particles.

This process forms the second 'subsurface' layer in the shell of the metal particles with the composition different from that of the surface (Fig. 3d). Complete oxidation of the chromium metal particles is, apparently, prevented by the formation of amorphous intermetallides at the boundaries of the grains, which are stable to oxidation: Cr_2Al_5—at 350–380 °C and Cr_2Al at 800 °C [2]. So, the decrease of the chromium grain size and consequent growth of the total grain boundary (Table 1) intensify the peaks related to chromium metal relative to those of chromium oxide Cr_2O_3 (Fig. 1).

For the loose 'nanocomposite' particles, the mechanism of oxidation by oxygen from the air appears to be different. Initially, the aluminium metal particles undergo additional oxidation. It is particularly accelerated at the aluminium melting point (660 °C) [28]. The oxidation of the chromium particles begins at higher temperatures [2]. However, it is known that the oxidation of metals is limited by diffusion [29]. So, the oxygen mobility in the formed oxide is of decisive importance. The oxygen mobility in aluminium oxide is substantially lower than that in transition metal oxides [30]. So, the alumina particles formed at lower temperatures hinder the chromium oxidation taking place at higher temperatures. We believe that this is the main reason why chromium oxides in lower oxidation degrees not observed before are formed in this system. At higher oxidation rates, these intermediate oxidation states of chromium are not stable, quickly undergoing deeper oxidation. The observed growth of the amount of the nitride-like chromium oxide phase relative to that of Cr_2O_3 at longer MA of the initial powder (Fig. 1) prove that the 'nanocomposite' and 'homogeneous' particles are formed in parallel during MA, at least, under our experimental conditions.

The formation of cavities in the metal particles is a separate problem. These cavities might be formed when aluminium is melted on the surface and oxidized. However, they are usually formed at the metal/oxide boundary [31]. The formation of some ordered Cr_4Al or Cr_2Al phases with the density exceeding that of the amorphous phases is the most likely reason.

Thus, different elements of the oxide matrix cermets with a complex microstructure are formed at different synthesis stages.

Conclusion

The cermet prepared by mechanical alloying of chromium and aluminium (20 wt%) powders followed by hydrothermal treatment at 100 °C and calcination at 1100 °C has very complex microstructure. It has the following characteristic features:

(1) Mechanically strong contacts between the particles are formed by oxide matrix. Two types of cores are observed randomly distributed in the oxide matrix. The 'homogeneous' cores predominantly consist of chromium metal with internal pores and layers of chromium–aluminium alloy located at the chromium grain boundaries. The 'nanocomposite' cores consist of mixed particles of alumina and chromium oxides.
(2) Chromium oxide phases with nitride-like structure and supposed stoichiometry CrO and Cr_2O are located in the 'nanocomposite' cores.
(3) The relations between different stages of the cermet preparation and design were discussed. The powder MA stage was found to be the most important for the cermet microstructure.

The combination of the oxide matrix with dispersed metal component improves the mechanical strength and increases the thermal conductivity of the cermet compared to traditional highly porous oxides. In comparison with traditional porous metals, CrAl cermets are more resistant to high-temperature oxidation. Finally, the synthesized cermet monolith has sufficiently high mechanical strength ($\sim$20 MPa) and porosity ($\sim$42%) with large pores (1–10 μm) to be used as a catalyst or membrane support.

Acknowledgements This work was supported in part by INTAS 06-1000005-7663 Project.

References

1. Yun YH, Hong WS, Choi SC (2002) J Mater Sci Lett 21:1297
2. Kim S, Kwon Y, Golubkova G, Lomovskii O, Dudina D, Dovlitova L, Malakhov V, Tikhov S, Usoltsev V, Sadykov V (2008) Inorg Mater 44:591
3. Tikhov S, Usoltsev V, Sadykov V, Pavlova S, Snegurenko O, Gogin L, Vostrikov Z, Salanov A, Tsybulya S, Litvak G, Golubkova G, Lomovskii O (2006) Stud Surf Sci Catal 161:641
4. Kositsina I, Kabanova I (2003) Russ Chem Bull 67:944
5. Goncharov O (2004) Inorg Mater 40:1476
6. Goncharov O, Kanunnikova O (2007) Inorg Mater 43:488
7. Suzuki T, Majime H, Hirai M, Suematsu H, Jiang W, Yatsui K (2002) Thin Solid Films 407:118
8. Desmoulins-Krawiec S, Aimonier C, Loppinet-Serani A, Weill F, Gorsse S, Etourneau J, Cansell F (2004) J Mater Chem 14:228
9. PC PDFWIN 06-0694
10. PC PDFWIN 35-0803
11. PC PDFWIN 11-0065
12. Tokoro H, Fujii S, Oku T (2004) J Mater Chem 14:253
13. High resolution spectra of inorganic and related compounds (1965) Sadtler Research Laboratories Inc. Philadelphia Penna 19104: Y207
14. Anderson EdA (1973) The Raman effect. Applications, vol 2. Marcel Dekker Inc, New York

15. Nakamoto K (1986) Infrared and Raman spectra of inorganic and coordination compounds. Wiley, New York
16. Zhang W, He Y, Zhang M, Yin Z, Chen Q (2000) J Phys D 33:912
17. Russel C (1992) J Mater Sci Lett 11:774
18. Ustinovschikov Yu, Pushkarev B (1999) Metals 2:52 (in Russian)
19. PC PDFWIN 08-0254
20. Wilhelmi K (1968) Acta Chem Scand 22:2565
21. Yelsukov E, Dorofeev G (2006) In: 5th international conference on mechanochemistry @ mechanical alloying (INCOME-2006) program and abstracts. Russia Novosibirsk. Inst. Solid State Chem. Mechanochem. 55
22. Maione A, Ruiz P (2006) Stud Surf Sci Catal 162:681
23. Wang D, Tong J, Xu H, Matsumura Y (2004) Catal Today 93–95: 689
24. Bai H Y, Michaelsen C, Gente C, Bormann R (2000) Phys Rev 63:064202-1-10
25. Kaloshkin SD (2000) J Metast Nanocryst Mater 8:591
26. Gaffet E, Bernard F (2003) J Metast Nanocryst Mater 15–16:259
27. Sadykov VA, Parmon VN, Tikhov SF (2009) Compos Interfaces 16:457
28. Anathapadmanabhan PV, Thiyagarajan TK, Sreekumar KP, Venkatramani N (2004) Scripta Mater 50:143
29. Mennicke C, Schuman E, Hussey RJ, Sproule GI, Graham MJ (1998) Oxid Metals 49:455
30. Boreskov GK (1982) In: Anderson JR, Boudart M (eds) Science and technology, vol 3. Springer Verlag, Berlin
31. Hou PY, Zhang XF, Cannon RM (2004) Scripta Mater 50:45